

Large deviation statistics of non-equilibrium fluctuations in a sheared model-fluid

Pritha Dolai and Aditi Simha

Department of Physics, Indian Institute of Technology Madras, Chennai 600036, India

E-mail: pritha@physics.iitm.ac.in and phyadt@iitm.ac.in

Abstract. We analyse the statistics of the shear stress in a one dimensional *model fluid*, that exhibits a rich phase behaviour akin to real complex fluids under shear. We show that the energy flux satisfies the Gallavotti-Cohen FT across all phases in the system. The theorem allows us to define an effective temperature which deviates considerably from the equilibrium temperature as the noise in the system increases. This deviation is negligible when the system size is small. The dependence of the effective temperature on the strain rate is phase-dependent. It doesn't vary much at the phase boundaries. The effective temperature can also be determined from the large deviation function of the energy flux. The local strain rate statistics obeys the large deviation principle and satisfies a fluctuation relation. It does not exhibit a distinct kink near zero strain rate because of inertia of the rotors in our system.

Keywords: Large deviations in non-equilibrium systems, fluctuation phenomena, stochastic particle dynamics, numerical simulations.

Contents

1	Introduction	2
2	Model and phase behaviour	3
3	Stress fluctuations and the fluctuation theorem	5
3.1	Variation of effective temperature	8
3.2	Effective temperature from the large deviation function	9
3.3	Statistics of the local strain rate	10
4	Conclusions	12

1. Introduction

The first quantitative statement of heat production in finite systems was provided by the Fluctuation theorem (FT) of Evans, Cohen and Morris in 1993 [1]. The theorem relates the probabilities of observing a positive value of the time averaged dissipative flux and a negative one of the same magnitude in a thermostatted dissipative system. It was first demonstrated in a molecular dynamics simulation of a sheared two-dimensional fluid of hard disks [1].

Several classifications of the FT exist. The *steady state* and *transient* FTs differ in the ensemble of trajectory segments considered. In the stationary state Fluctuation theorem (SSFT), such as in the original work of Evans *et al* [1], the trajectories of fixed duration τ belong to the driven steady state and the FT becomes valid in the limit $\tau \rightarrow \infty$. In the transient FT (TFT) [2], the segments belong to a system initially in an equilibrium state evolving into a non-equilibrium steady state [3].

Another classification is based on whether the fluctuation statistics are for a *global* or *local* quantity. The FT of Evans *et al* was for fluctuations in the total entropy production which is a global quantity. Gallavotti and Cohen [4, 5] provided a rigorous mathematical derivation of this theorem and in addition rederived a FT for the average of local observables. This local FT is easier to test experimentally as negative fluctuations, too rare to be observed experimentally in global quantities, are more prevalent in local quantities. Moreover, it does not require steady state conditions to hold globally and can be applied when it holds only locally.

To put our work in context, it is essential to distinguish between the FT of Evans and Searles [3] and that of Gallavotti and Cohen [4, 5]. The former is a statement of fluctuations in the dissipative flux of thermostatted non-equilibrium states. It provides an expression for the probability of a dissipative flux in the direction opposite to that required by the second law of thermodynamics. It requires that the initial state or distribution satisfies the condition of ergodic consistency. The Gallavotti-Cohen FT [4, 5] is more general and applies to non-equilibrium systems driven far from equilibrium into nonlinear chaotic regimes. It depends crucially on the Chaotic Hypothesis which imposes certain conditions on systems to which it can be applied. Our system which is a dissipative stochastic system driven far from equilibrium falls under this category. We show that the energy flux averaged over a duration τ , W_τ , satisfies the Gallavotti-Cohen FT

$$\lim_{\tau \rightarrow \infty} \frac{1}{\tau} \ln \frac{P(+W_\tau)}{P(-W_\tau)} = \beta W_\tau \quad (1)$$

in the steady state. $\beta = (k_B T_{eff})^{-1}$ defines an effective temperature.

Both FTs have been validated in several systems. The Evans-Searles FT has been verified in a number of molecular dynamics simulations, electrical resistor circuits [8], and for a colloidal particle in an optical trap [6, 7]. The Gallavotti-Cohen FT has been satisfied in many real systems such as in turbulent flows [9–11], turbulent Rayleigh-Bénard convection [12], vertically agitated granular gas [13] and in a sheared micellar

Large deviation statistics of non-equilibrium fluctuations in a sheared model-fluid gel [14].

Our system mimics a fluid under shear at constant strain rate and exhibits a rich phase behaviour similar to that seen in real complex fluids under shear [15]. Unlike in the isoenergetic simulations of a sheared two dimensional fluid [1], the heat and energy flux have different statistics in our system and the dynamics is not time reversal invariant. We show that eqn.(1) is satisfied in all phases of the system and study the variation of the effective temperature, T_{eff} , with the strain rate, strength of the stochastic force and relation to changes in phase. We show that T_{eff} can also be obtained from the large deviation function (LDF) of the energy flux. Finally, we analyse the statistics of fluctuations in the local strain rate.

2. Model and phase behaviour

Our *model fluid* is the classical one-dimensional XY model of a lattice of spins or rotors (Figure 1), each of which can rotate perpendicular to the lattice. The angle θ_i of the spin $\mathbf{s}_i = (\cos \theta_i, \sin \theta_i)$ is the only degree of freedom of each rotor or spin. Each spin interacts only with its nearest neighbours via torsional forces. In the equilibrium model these are forces arising from the interaction potential $U = -\sum_1^{N-1} \mathbf{s}_i \cdot \mathbf{s}_{i+1}$.

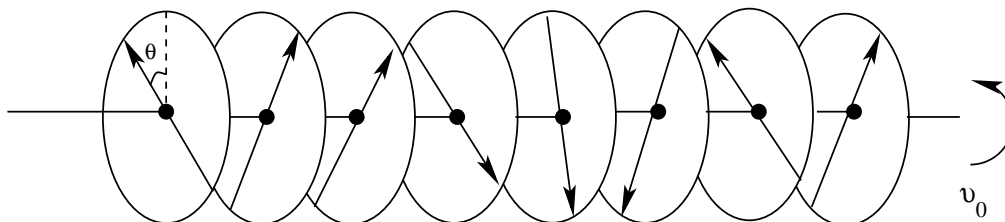


Figure 1. The 1D driven XY model. The angle θ and velocity $\dot{\theta}$ of each rotor characterizes the state of the system at each instant.

To generate the non-equilibrium steady states of this model, the rotors are subjected to Langevin dynamics. In addition to the conservative force given by U , frictional and stochastic forces are included that conserve total angular momentum. The net torsional force on each rotor determines its angular acceleration according to Newton's law of motion, *i.e.*,

$$I\ddot{\theta}_i = \tau_i = \tau_{i,i+1} + \tau_{i,i-1}, \quad (2)$$

where I is the moment of inertia of each rotor which is unity in the chosen units and τ_i the total torque acting on rotor i . This has three contributions: conservative, dissipative and random, each of which is pairwise additive and acts along $\hat{\theta}_{ij}$ where $\theta_{ij} = \theta_i - \theta_j$ is the relative angular separation between rotors i and j .

$$\tau_i = \sum_{\langle ij \rangle} \tau_{ij}^C + \tau_{ij}^D + \tau_{ij}^R \quad (3)$$

Large deviation statistics of non-equilibrium fluctuations in a sheared model-fluid

The conservative torque, $\tau_i^C = -\frac{\partial U(\theta_{ij})}{\partial \theta_i}$. The frictional torque depends only on the relative velocity between rotors and has the simple form $\tau_{ij}^D = -\Gamma(\dot{\theta}_i - \dot{\theta}_j)$ where Γ is the frictional co-efficient. The random torque $\tau_{ij}^R = \sigma \zeta_{ij}$, where σ is the amplitude of the random torque and ζ_{ij} is a Gaussian random variable of unit variance. The system is driven by rotating one of its boundaries relative to the other. This is done using Lees-Edwards boundary condition for the angle variable which allows us to impose a relative velocity v_0 between the boundaries of the system along with periodic boundary conditions so that edge effects are eliminated. The imposed strain rate is defined as $\dot{\gamma} = v_0/N$, where N is the number of rotors. The model has been used earlier to measure transition rates in non-equilibrium steady states and its rich phase behaviour likened to the phenomenology of real complex fluids under shear [15–17]. A model that bears some similarity to ours is the sheared solid model [18].

The equations of motion (2) are integrated forward in time using a self-consistent Dissipative Particle Dynamics (DPD) algorithm [19, 20]. The time step of integration dt is chosen such that the relative motion between rotors per time step is not greater than 0.24.

The system exhibits four qualitatively distinct phases. Figure 2(a) depicts the various phases observed as a function of the imposed strain rate, $\dot{\gamma}$ and noise amplitude (expressed in terms of $T_0 = \sigma^2/2\Gamma$) for fixed $\Gamma = 0.04$. We distinguish between these phases based on the distribution of the time-averaged local strain rate ($\langle d\theta_{i,i+1}/dt \rangle$) in the system. The following four phases are observed : (I) Uniform shear phase - the average local shear rate is the same through out the system. This phase exists at high σ and $\Gamma\dot{\gamma}$ where thermal and frictional forces are much larger than the conservative force $\partial U(\theta_{ij})/\partial \theta_i$. Uniform shear implies a linear average velocity profile. All Newtonian fluids shear uniformly. In complex fluids, a uniform shear flow regime always exists (Figure 2(b)). (II) Slip plane phase - the shear in this phase is localized to a few neighbouring rotors (or planes) while the majority move without any relative motion between their neighbours as in a elastic solid (Figure 2(d)). This phase is observed when the thermal energy is small and the average torque is less than the maximum potential gradient. Relative motion at the slip plane produces an oscillatory torque that propagates in the solid region as damped torsional waves. Slip planes have been observed in surfactant cubic phases [21]. (III) Solid-fluid coexistence - This phase is created when the yield event at a slip plane triggers more yeild events locally giving rise to a finite region thats fluid (where the rotors overcome the potential barrier), co-existing with solid regions (Figure 2(e)). This co-existence is possible only when the local time averaged stress is just below the yield point. Such phases have been observed in foams [22, 23]. (IV) Shear banding - the local shear rate assumes two or more values, forming regions of different effective viscosities (Figure 2(c)). Each of these regions is called a band. Shear banding has been observed in polymers [24, 25]. A precise characterization of these phases along with a mean field analysis of the model's phase behaviour can be found in [15].

For the range of $\dot{\gamma}$ and σ studied (at fixed value of $\Gamma = 0.04$), we do not see a

Large deviation statistics of non-equilibrium fluctuations in a sheared model-fluid

turbulent phase in this system. However, we expect to see turbulence for large $\dot{\gamma}$, large system size, and by reducing the value of the frictional co-efficient Γ .

We restrict our study here to properties of the driven steady state which is attained after an initial transient behaviour. In the steady state, the rate of change of the total energy $\dot{E} = W - \dot{Q}$, where the energy flux or power W is the rate at which work is done on the system by the driving force and the heat flux \dot{Q} is the heat dissipated per unit time. Since the system is sheared at constant strain rate, $W(t) = f(t)v_0$ where f is the net torque between neighbouring rotors on either side of the sheared boundary. The distribution of f is therefore the distribution of the shear stress in the system. The frictional coefficient and the interaction potential are kept fixed in our simulations while the strain rate ($\dot{\gamma}$) and noise amplitude (σ) are varied.

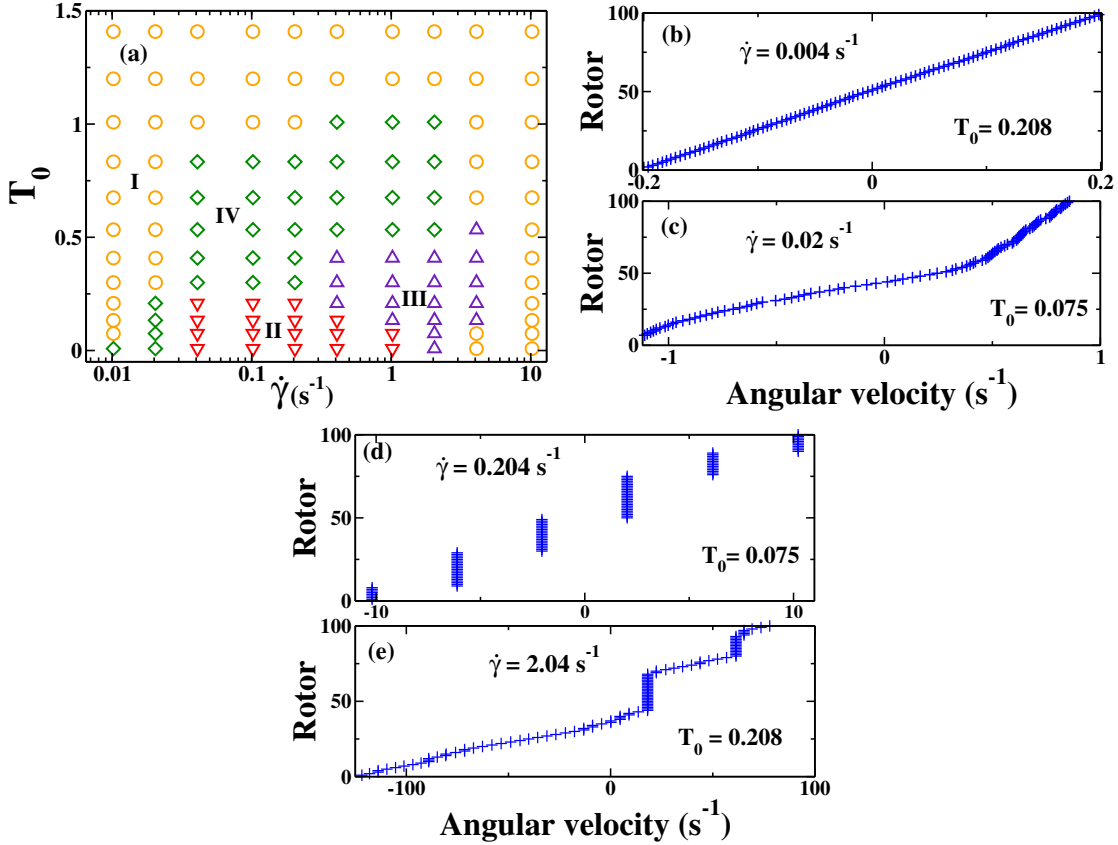


Figure 2. (a)Phase diagram of the model fluid for $\Gamma = 0.04s^{-1}$ and $I = 1$ indicating four distinct phases. (I) uniform shear phase, (II) slip-planes, (III) solid-fluid coexistence, (IV) shear banding. Average velocity profile in - (b) Phase I, (c) Phase IV, (d) Phase II and (e) Phase III.

3. Stress fluctuations and the fluctuation theorem

The shear stress of the system fluctuates about a positive mean value and assumes both positive and negative values. Shown in Figure 3(a) is a typical time evolution

Large deviation statistics of non-equilibrium fluctuations in a sheared model-fluid

of the shear stress f_τ averaged over duration τ for a system of 100 rotors in the shear banding phase. To find the probability distribution $P(f_\tau)$, $f(t)$ is recorded as the system evolves in the steady state over a long duration of time (corresponding to a few hundred revolutions of each rotor) and over many realizations of the random torque. $2\pi/\dot{\gamma}$, which is the time it takes for a rotor experiencing a local shear rate $\dot{\gamma}$ to complete one revolution, defines a timescale. The data is then averaged over different durations τ larger than any correlation time (t_c) in the system. In some cases the window of averaging is shifted from a previous one by a time larger than the correlation time to improve sampling. The distribution of the resulting averaged data is $P(f_\tau)$. The average energy flux into the system in a duration τ is $W_\tau = \frac{1}{\tau} \int_t^{t+\tau} W(t') dt' = f_\tau v_0$; and $P(W_\tau/v_0) = P(f_\tau)$. We define the dimensionless quantity $X_\tau = W_\tau/\langle W_\tau \rangle$. The distribution $P(X_\tau)$ for different values of τ corresponding to the fluctuations in Fig. 3(a) is shown in Fig. 3(b). Its deviation from a Gaussian distribution is shown in the inset.

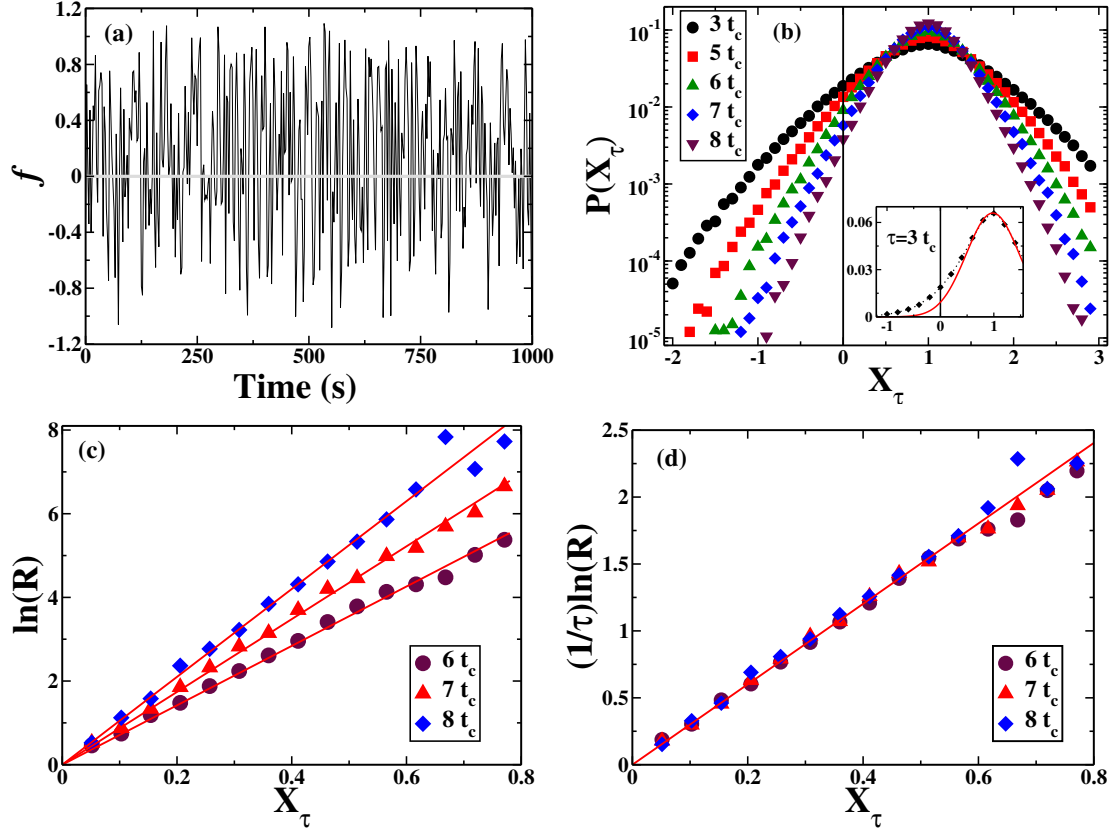


Figure 3. (a) Typical shear-stress fluctuations for $\dot{\gamma}=0.327 \text{ s}^{-1}$, $\sigma = 0.1$. (b) Corresponding probability distribution functions of X_τ for different τ 's. (c) Plot of $\ln[P(+X_\tau)/P(-X_\tau)]$ vs X_τ for different durations τ expressed in terms of the correlation time t_c . Solid lines are the straight line fits to data. (d) Plot of $\frac{1}{\tau} \ln[P(+X_\tau)/P(-X_\tau)]$ vs X_τ . All collapse into a straight line passing through the origin as shown by the fitted solid line.

In terms of X_τ , eq.(1) for finite τ is

$$\ln(R) \equiv \ln \frac{P(+X_\tau)}{P(-X_\tau)} = \beta \langle W_\tau \rangle X_\tau \tau. \quad (4)$$

We set $k_B = 1$. The straight lines in Fig. 3(c) validate this and their collapse onto one line on scaling with $1/\tau$ (Fig. 3(d)) validates eqn. (1). T_{eff} can be calculated from the slope of the collapsed line. It quantifies the probability of observing negative shear in the system; a large T_{eff} corresponds to a higher probability of finding the system with negative shear stress.

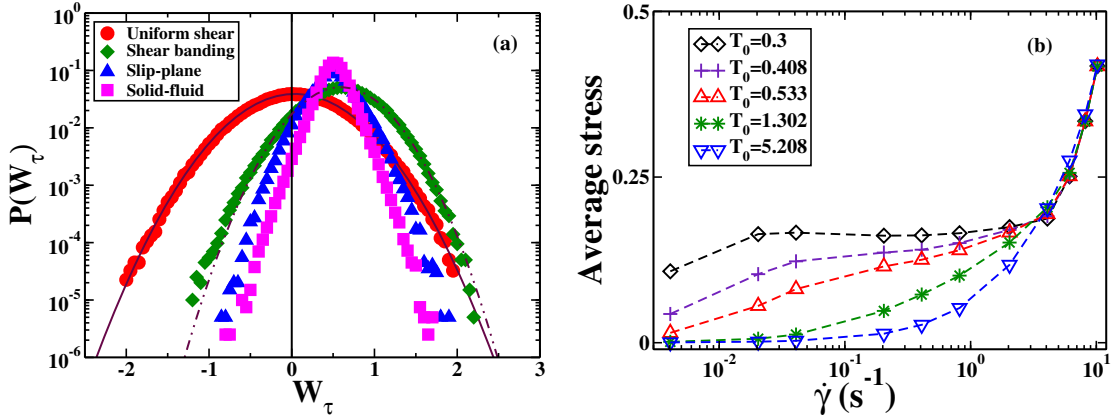


Figure 4. (a) Probability distributions in different phases. The distributions in uniform shear flow, shear banding, slip-plane and solid-fluid co-existence phase correspond to following sets of parameters: (i) $T_0 = 0.675$, $\dot{\gamma} = 0.004s^{-1}$, $t_c = 4.1 s$. (ii) $T_0 = 0.208$, $\dot{\gamma} = 0.102s^{-1}$, $t_c = 4.4 s$. (iii) $T_0 = 0.133$, $\dot{\gamma} = 0.122s^{-1}$, $t_c = 3.4 s$. (iv) $T_0 = 0.133$, $\dot{\gamma} = 1.22s^{-1}$, $t_c = 1.7 s$. (b) Average stress as a function of $\dot{\gamma}$ for different T_0 .

When the fluctuations are Gaussian distributed, the probability distribution $P(W_\tau) \propto \exp -(W_\tau - \langle W_\tau \rangle)^2 / (2\sigma_{W_\tau}^2)$. This would then imply

$$\frac{P(+W_\tau)}{P(-W_\tau)} = \exp (2\langle W_\tau \rangle W_\tau / \sigma_{W_\tau}^2). \quad (5)$$

Comparing this with the ratio of the probabilities according to the Gallavotti-Cohen FT (1), we get

$$\begin{aligned} 2\langle W_\tau \rangle / \sigma_{W_\tau}^2 &= \beta \tau \\ \Rightarrow \sigma_{W_\tau} / \langle W_\tau \rangle &= \sqrt{2T / \langle W_\tau \rangle \tau} \end{aligned} \quad (6)$$

The left hand side (LHS) is a quantity that involves the standard deviation and mean of the Gaussian distribution. The temperature T is the thermodynamic temperature when the system is in the linear response regime. It is the effective temperature, T_{eff} , when the system is not in the linear response regime and the fluctuations are Gaussian distributed. The quantity on the LHS of (6) is also related to the curvature of the LDF at its minimum and its derivative at $W_\tau = 0$ for Gaussian fluctuations. We test if this relation holds generally when the fluctuations are not Gaussian in Sec.3.2.

The probability distribution for W_τ in the various phases is shown in Fig. 4(a). The distribution at large noise amplitudes (shown by red filled circles) is Gaussian. The distribution in the shear banding phase is nearly Gaussian but deviates from it far away from the mean. It is non-Gaussian in the slip-plane and two phase or coexistence regime.

The variation of average stress with strain rate for different T_0 is shown in Fig. 4(b). For small T_0 , the average stress plateaus before increasing sharply with $\dot{\gamma}$. This plateau region indicates the shear banding regime which diminishes with increasing T_0 . For large T_0 , the average stress increases very slowly for small $\dot{\gamma}$ before increasing sharply for $\dot{\gamma} > 2.0 s^{-1}$. Beyond $\dot{\gamma} = 4.0 s^{-1}$ curves for different T_0 fall on each other in the uniform shear flow regime.

3.1. Variation of effective temperature

The variation of T_{eff} with strain rate $\dot{\gamma}$ for a fixed noise amplitude, $\sigma = 0.1$, is shown in Fig. 5(a). In the range of $\dot{\gamma}$ covered, the system goes through three different phases (boundaries shown by vertical dashed lines) as can be inferred from the phase diagram; the uniform shear regime up to $\dot{\gamma} = 0.02 s^{-1}$, shear banding between $\dot{\gamma} = 0.02 - 0.4 s^{-1}$, and the solid-fluid co-existence at higher $\dot{\gamma}$. Its variation with $\dot{\gamma}$ is different in each phase. The effective temperature shows a very slow increase with $\dot{\gamma}$ in uniform shear flow. In the shear banded phase it increases as $\sqrt{\dot{\gamma}}$ and much faster in the coexistence phase. At the phase boundaries T_{eff} does not vary much.

The effective temperature is plotted along with the average interaction energy, $\langle PE \rangle$ and the standard deviation of the total energy, δE , in Fig. 5(b). The variation of T_{eff} is qualitatively similar to δE . It is proportional to δE in each of the phases albeit with a different constant of proportionality.

We present our results for the variation of the effective temperature with the noise amplitude, σ , in terms of $T_0 = \sigma^2/2\Gamma$, the temperature at equilibrium given by the Fluctuation Dissipation Theorem for the same σ . Fig. 5(c) shows how T_{eff} varies with T_0 for systems of size $N = 10$ and $N = 100$. At $N = 10$, we find that $T_{eff} \approx T_0$ as indicated by the black solid line corresponding to $T_{eff} = T_0$. This is not true as the system size increases where it deviates considerably from T_0 even when the strain rate is small. The weak dependence for small N suggests a crossover length ($L = N_0$) below which nothing happens.

An analysis of the system size dependence of T_{eff} , for fixed values of σ and $\dot{\gamma}$, indicates that it increases linearly with system size (see Fig. 5(d)). We speculate that this is due to the driving speed, $v_0 = \dot{\gamma}N$, which increases linearly with N . Plotted in the inset is T_{eff}/N vs. N , which is nearly constant.

Except in the region corresponding to very low noise amplitudes ($\sigma < 0.08$), we have been able to show that the Gallavotti-Cohen FT is satisfied. We speculate that at these noise amplitudes the system does not sample enough of the phase space in realistic time.

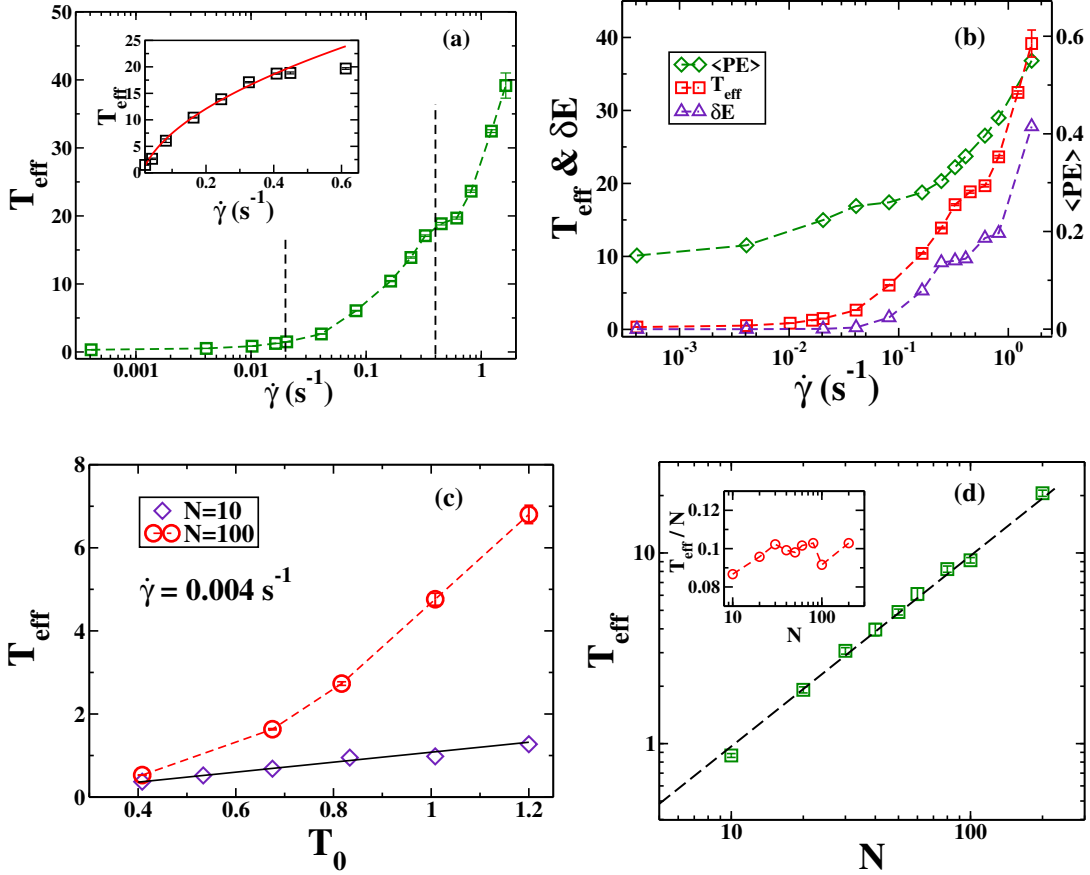


Figure 5. (a) T_{eff} as a function of $\dot{\gamma}$ for fixed noise amplitude $\sigma=0.1$. In the shear banding regime the curve is fitted to $\dot{\gamma}^{1/2}$ as shown in inset. The vertical lines indicate the boundary between different phases. (b) Standard deviation in energy, average potential energy and T_{eff} as a function of $\dot{\gamma}$. (c) Variation of effective temperature (T_{eff}) with (T_0) for a fixed strain rate $\dot{\gamma}=0.004$ s $^{-1}$ for $N = 10$ and 100 . Black solid line indicates the corresponding equilibrium temperature T_0 . (d) T_{eff} increases linearly with the system size. Inset: T_{eff}/N as a function of N .

3.2. Effective temperature from the large deviation function

The effective temperature for Gaussian fluctuations can be calculated from eq.(6) if the mean and standard deviation of the distribution are known. Here we relate it to quantities in the large deviation function, its curvature and slope at $W_\tau = 0$. We define the dimensionless quantity $X_\tau = W_\tau / \langle W_\tau \rangle$. X_τ has the distribution,

$$P(X_\tau) = \exp[-(X_\tau - 1)^2 / 2 (\sigma_{W_\tau} / \langle W_\tau \rangle)^2], \quad (7)$$

where $\langle W_\tau \rangle$ and σ are the mean and standard deviation, respectively, of the distribution of W_τ . The LDF of X_τ is then

$$I(X_\tau) = - \lim_{\tau \rightarrow \infty} \frac{1}{\tau} \ln P(X_\tau) = \lim_{\tau \rightarrow \infty} \frac{1}{\tau} \frac{(X_\tau - 1)^2}{2 (\sigma_{W_\tau} / \langle W_\tau \rangle)^2} \quad (8)$$

Therefore,

$$I'(X_\tau = 0) = -(\langle W_\tau \rangle / \sigma_{W_\tau})^2 / \tau, \quad I''(X_\tau = 1) = (\langle W_\tau \rangle / \sigma_{W_\tau})^2 / \tau \quad (9)$$

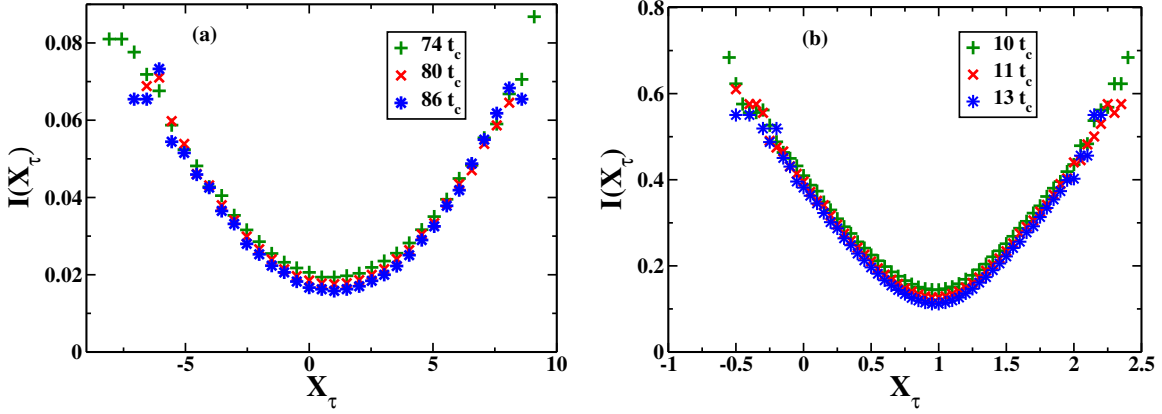


Figure 6. (a) LDF of X_τ for Gaussian fluctuations for $\sigma = 0.15$ and $\dot{\gamma} = 0.004s^{-1}$. (b) LDF for non-Gaussian fluctuations for $\sigma = 0.1$ and $\dot{\gamma} = 0.327s^{-1}$.

Both the curvature at the minima and the slope at $X_\tau = 0$ of the LDF are the same, except for a difference in sign, and give the ratio of the mean to the standard deviation of the original distribution of W_τ . Eq.(6) can be rewritten in terms of these quantities as

$$\frac{2T}{\langle W_\tau \rangle} = \frac{-1}{I'(X_\tau = 0)}, \quad (10)$$

$$\frac{2T}{\langle W_\tau \rangle} = \frac{1}{I''(X_\tau = 1)}. \quad (11)$$

Using the LDF for X_τ , we have used eqs. (10,11) to calculate T for the following two cases:

(i) $P(X_\tau)$ is Gaussian - $\dot{\gamma} = 0.004 s^{-1}$, $\sigma = 0.15$, $I'(X_\tau = 0) = -0.002 = -I''(X_\tau = 1)$. This yields an effective temperature $T_{eff} = 1.667$. Our earlier result for the same parameters is 1.63.

(ii) $P(X_\tau)$ is non-Gaussian - $\dot{\gamma} = 0.327 s^{-1}$, $\sigma = 0.1$, $I'(X_\tau = 0) = -0.38$, $I''(X_\tau = 0) = -0.79$. Eq.(10) gives $T_{eff} = 17.0$. The effective temperature obtained from the FT is 17.09. The LDFs for the above two cases are plotted in Fig. 6. We find that the effective temperature can be obtained from the derivative of the LDF at $W_\tau = 0$.

3.3. Statistics of the local strain rate

The mean strain rate, $\dot{\gamma}$, imposed at the boundaries is constant in time but the local strain rate $\dot{\gamma}_i$ between neighbouring rotors i and $i + 1$ is a fluctuating quantity. We find the probability distribution $P(\dot{\gamma}_\tau)$ of $\dot{\gamma}_i$ averaged over rotors and duration τ . We define the large deviation function (LDF) for the strain rate, $F(\dot{\gamma}_\tau) \equiv \lim_{\tau \rightarrow \infty} -(1/\tau) \ln P(\dot{\gamma}_\tau)$ and show that it exists (Fig. 7(a)). The antisymmetric part of the LDF (Fig. 7(b)) obeys a fluctuation relation *i.e.*, $F(\dot{\gamma}_\tau) - F(-\dot{\gamma}_\tau) \propto \tau \dot{\gamma}_\tau$ (Fig. 7(c)). These plots are for $\sigma = 0.13$, $\dot{\gamma} = 0.04 s^{-1}$.

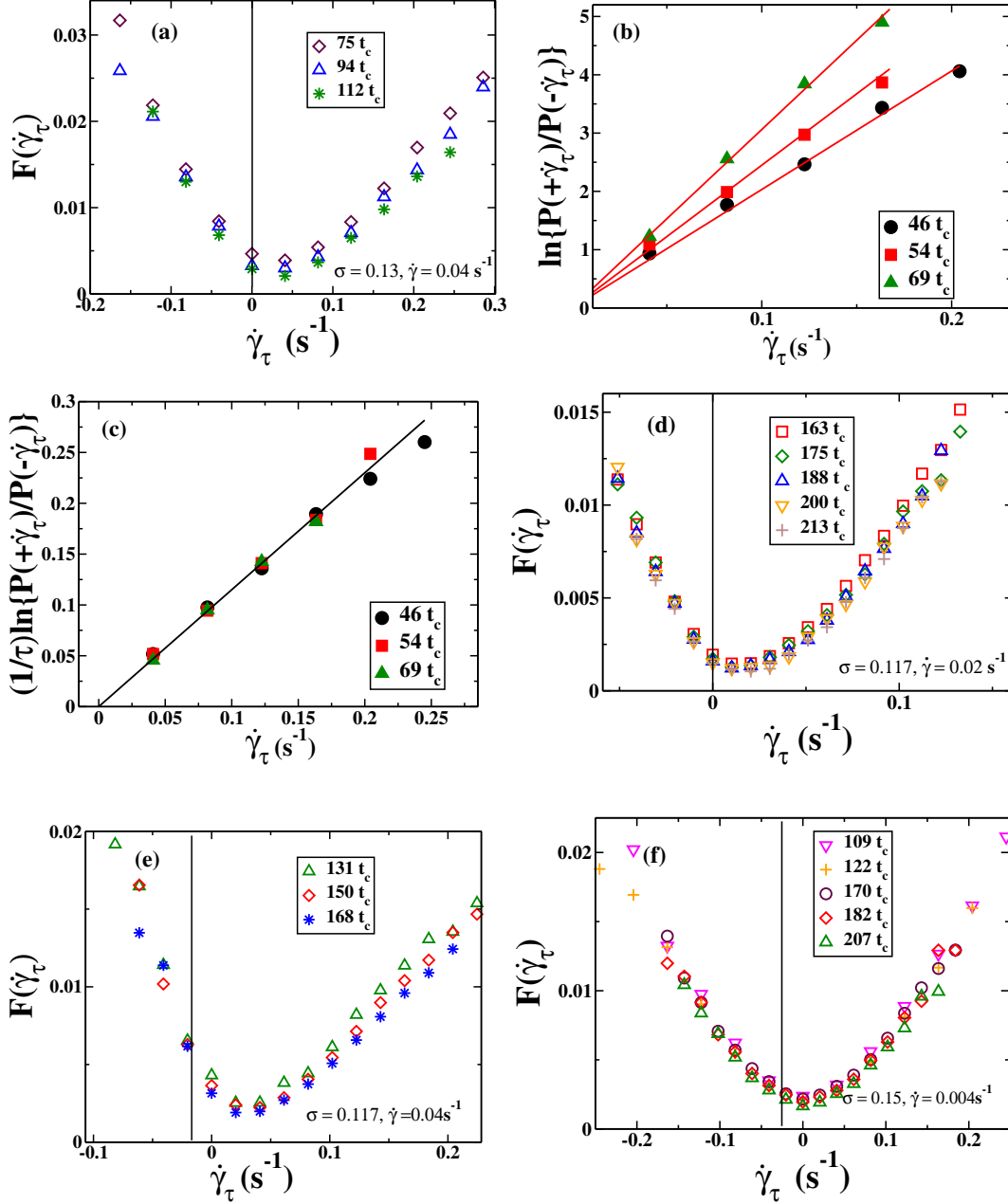


Figure 7. (a) The LDF for the local strain rate for parameter values $\sigma = 0.13$ and $\dot{\gamma} = 0.04 \text{ s}^{-1}$. (b) Plot of $\ln\{P(+\dot{\gamma}_\tau)/P(-\dot{\gamma}_\tau)\}$ vs $\dot{\gamma}_\tau$ for different τ expressed in terms of t_c for same set of parameter values. The solid lines are the straight line fits to data. (c) All these lines of $\ln\{P(+\dot{\gamma}_\tau)/P(-\dot{\gamma}_\tau)\}$ vs $\dot{\gamma}_\tau$ collapse into a single straight line passing through the origin on scaling by $\frac{1}{\tau}$, shown by the fitted solid line. (d) The LDF for parameter values $\sigma = 0.117$ and $\dot{\gamma} = 0.02 \text{ s}^{-1}$. (e) The LDF for $\sigma = 0.117$ and $\dot{\gamma} = 0.04 \text{ s}^{-1}$. (f) The large deviation function for $\sigma = 0.15$ and $\dot{\gamma} = 0.004 \text{ s}^{-1}$. $t_c \approx 4 \text{ s}$ in all the plots above.

LDFs are plotted for 3 other sets of parameters. Fig. 7(d) and Fig. 7(e) show LDFs for $\dot{\gamma} = 0.02 \text{ s}^{-1}$ and $\dot{\gamma} = 0.04 \text{ s}^{-1}$, respectively, with σ kept constant at 0.117. Larger the strain rate $\dot{\gamma}$, more asymmetric the LDF because of the rarity of negative

Large deviation statistics of non-equilibrium fluctuations in a sheared model-fluid fluctuations. The LDF for $\sigma = 0.15$ and $\dot{\gamma} = 0.004 \text{ s}^{-1}$ is plotted in Fig. 7(f). This LDF is almost symmetric around zero strain rate because of the large noise amplitude. There is no distinctly visible kink at $\dot{\gamma}_\tau = 0$ in any of the three LDFs. We speculate that this is because of inertia of the rotors. A kink in the LDF has been observed earlier for entropy production in [26], and for the velocity of a self-propelled polar particle in [27]. In [26], the kink was attributed to a dynamical cross-over between a regime of high entropy production and a regime of low entropy production. In [27], the kink is visible because the dynamics of particles is overdamped and inertia is completely ignored. The higher the strain rate, the greater the asymmetry of the LDF about the minimum. A more detailed study of the LDF for the local strain rate is currently under way.

4. Conclusions

We show that the Gallavotti-Cohen FT is satisfied across all phases of the sheared *model fluid* which exhibits phases similar to real complex fluids under shear. We study the dependence of the effective temperature T_{eff} (defined by the FT), on the strain rate, noise amplitude and system size. $T_{eff} \approx T_0$, the equilibrium thermodynamic temperature, at small strain rates. The linear response regime, when this happens, depends on the noise amplitude and system size. The larger the noise amplitude, the smaller the $\dot{\gamma}$ at which the linear response regime sets in. T_{eff} deviates considerably from T_0 as the noise amplitude increases (for fixed strain rate and system size). This deviation is negligible when the system size is small, suggesting that there is a crossover length (or system size) below which nothing happens. The dependence of T_{eff} on $\dot{\gamma}$ is phase-dependent. It doesn't change much at the phase boundaries. The effective temperature can also be determined from the derivative of the LDF for the energy flux at $W_\tau = 0$. The local strain rate statistics obeys the large deviation principle and satisfies a fluctuation relation. It does not exhibit a distinct kink at zero strain rate, seen in other systems [26, 27], because of the inertia of rotors in our system.

Acknowledgments

We thank R. M. L. Evans, Sriram Ramaswamy, Abhik Basu and S. Govindrajan for useful inputs and comments. We also thank P. B. Sunil Kumar for providing computing facilities.

References

- [1] D. J. Evans, E. G. D. Cohen and G. P. Morriss, Phys. Rev. Lett. **71**, 2401 (1993).
- [2] S.R. Williams, D. J. Searles and D. J. Evans, Phys. Rev. E **70**, 066113 (2004).
- [3] D. J. Evans and D. J. Searles, Phys. Rev. E **50**, 1645 (1994).

- [4] G. Gallavotti and E. G. D. Cohen, *Phys. Rev. Lett.* **74**, 2694 (1995).
- [5] G. Gallavotti and E. G. D. Cohen, *J. Stat. Phys.* **80**, 931 (1995).
- [6] D. M. Carberry, J. C. Reid, G. M. Wang, E. M. Sevick, Debra J. Searles and Denis J. Evans, *Phys. Rev. Lett.* **92**, 140601 (2004).
- [7] G. M. Wang, E. M. Sevick, Emil Mittag, Debra J. Searles and Denis J. Evans, *Phys. Rev. Lett.* **89**, 050601 (2002).
- [8] N. Garnier and S. Ciliberto, *Phys. Rev. E* **71**, 060101 (2005).
- [9] S. Ciliberto, C. Laroche, *J. Phys. IV (France)* **8**, 215 (1998).
- [10] S. Ciliberto, N Garnier, S Hernandez, C Lacpatia, J. F Pinton and G Ruiz Chavarria, *Physica (Amsterdam)* **340A**, 240 (2004).
- [11] M. M. Bandi, J. R. Cressman, and W. I. Goldburg, *J. Stat. Phys.* **130**, 27 (2008).
- [12] X. D. Shang, P. Tong and K. Q. Xia, *Phys. Rev. E* **72**, 015301 (2005).
- [13] K. Feitosa and N. Menon, *Phys. Rev. Lett.* **92**, 164301 (2004).
- [14] S. Majumdar and A. K. Sood, *Phys. Rev. Lett.* **101**, 078301 (2008).
- [15] R. M. L. Evans, Craig A. Hall, R. Aditi Simha and Tom S. Welsh, *Phys. Rev. Lett.* **114**, 138301 (2015).
- [16] R. M. L. Evans, R. A. Simha, A. Baule and P. D. Olmsted, *Phys. Rev. E* **81**, 051109 (2010).
- [17] R. M. L. Evans, *Contemporary Physics*, **51**, 413-427 (2010).
- [18] Rangan Lahiri and Sriram Ramaswamy, *Phys. Rev. Lett.* **73**, 1043 (1994).
- [19] Robert D. Groot and Patrick B. Warren, *J. Chem. Phys.* **107**(11) (1997).
- [20] I. Pagonabarraga, *Europhys. Lett.* **42**(4), 377-382 (1998).
- [21] J. L. Jones and T. C. B. McLeish, *Langmuir* **11**, 785 (1995).
- [22] K. Krishan and M. Dennin, *Phys. Rev. E* **78**, 051504 (2008).
- [23] G. Debrégeas, H. Tabuteau and J. M. di Meglio, *Phys. Rev. Lett.* **87**, 178305 (2001).
- [24] J. Cao and A. E. Likhtman, *Phys. Rev. Lett.* **108**, 028302 (2012).
- [25] I. Kunita, K. Sato, Y. Tanaka, Y. Takikawa, H. Orihara and T. Nakagaki, *Phys. Rev. Lett.* **109**, 248303 (2012).
- [26] Thomas Speck, Andreas Engel and Udo Seifert, *J. Stat. Mech.* P12001 (2012).
- [27] Nitin Kumar, Sriram Ramaswamy and A. K. Sood, *Phys. Rev. Lett.* **106**, 118001 (2011).